49. Phase-Change Optical Recording

The present chapter takes the reader from the basics of phase-change recording up to the latest achievements in the field. It discusses in detail the specific features of Te-based compounds that made them the best materials for phase-change data storage. It is demonstrated that the essence of phase-change recording does not consist of simple disordering of the medium through melting and subsequent quenching as previously believed but is due to a switch of Ge atoms between octahedral and tetrahedral symmetry positions within the Te face-centered cubic lattice. It is this nature of the transition that makes the Te-based media fast and stable. The chapter is concluded by the introduction of a concept of the super-resolution near-field structure (super-RENS) disc that allows the reduction of the bit size well below the diffraction limit and makes 100 GB/disc storage a reality.

49.1 **Digital Versatile Discs (DVDs)** 1140
49.1.1 Questions Pertaining to DVD Recording 1140
49.1.2 Local Structure and its Changes During the Phase Transition 1140
49.1.3 Related Issues 1143
49.2 **Super-RENS Discs** 1144
49.3 **In Lieu of Conclusion** 1145
References 1145

The idea of phase-change recording dates back to the mid 1960s when *Ovshinsky* [49.1] first suggested using differences in electrical and optical properties between amorphous and crystalline phases of Te-based chalcogenides for data storage. The idea of phase-change recording is quite simple.

When a melt is cooled down slowly, such that the structure always remains in thermal equilibrium, upon reaching the crystallization temperature the material crystallizes, i. e. is transformed into a solid state with a well-defined periodic structure. If, on the other hand, the cooling rate is fast, then at a certain temperature the viscosity of the liquid increases to a degree such that the structure can no longer relax following the changes in temperature; one obtains a supercooled liquid and then a glass. In contrast to the crystallization temperature, the glass-transition temperature is not well defined. A range of temperatures exist and the particular temperature of the glass transition depends on the cooling rate.

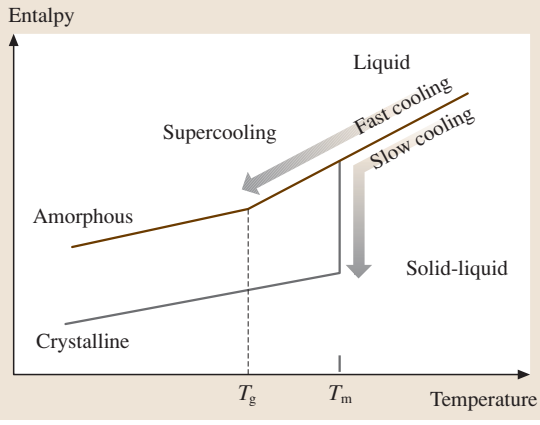

Fig. 49.1 A glass-formation diagram

Once in the solid state, the glass, if kept at a temperature close to the glass-transition temperature, crystallizes. On the other hand, rapid heating of the crystalline material to a temperature above the melting point and subsequent rapid cooling (quenching) can produce a glassy state. This glass-formation diagram is demonstrated by Fig. 49.1.

The material can also be heated by light. Exposure of an amorphous material to a laser light that heats it above the glass-transition temperature results in crystallization while short and intense laser pulses melt the material and—provided the heat-dissipation rate is fast enough—an amorphous recorded bit is formed.

49.1 Digital Versatile Discs (DVDs)

The latest commercial implementation of phase-change recording are rewritable digital versatile disks (DVDs) [49.2]. Various materials have been tried for potential use in phase-change memories and the best in terms of speed and stability are ternary Ge–Sb–Te (primarily $Ge_2Sb_2Te_5$, hereafter referred to as GST) and quaternary Ag–In–Sb–Te (AIST) alloys. The former are used in DVD random access memory (DVD-RAM) and the latter in DVD rewritable (DVD-RW) disks. While there are some differences in the device structure and recording strategies, both these kinds of rewritable DVDs are capable of storing up to 4.7 Gbits of information.

A basic disk structure consists of four layers (Fig. 49.2). The recording layer (GST or AIST) is sandwiched between Zn–SiO2 layers and a metallic Al–Cr layer serves as a reflection layer and also as a heat sink to ensure the rapid cooling necessary for the formation of the amorphous phase.

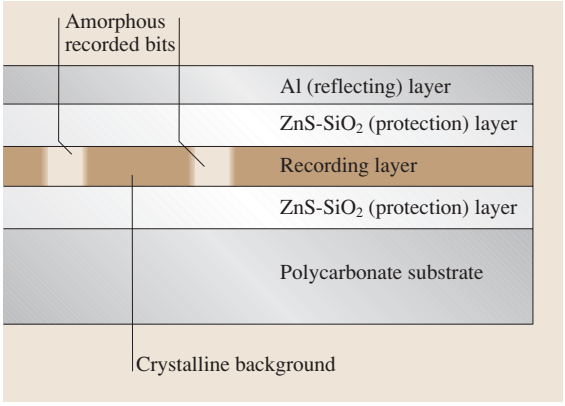

Fig. 49.2 A schematic representation of a DVD structure

49.1.1 Questions Pertaining to DVD Recording

While the phenomenology of phase-change recording is simple, the realistic nanoscale mechanism of the structural transformation has remained unclear for almost 30 years since the idea of phase-change recording was first suggested.

In particular, there are several fundamental questions that need to be answered. Interestingly, some of them have never been asked previously.

1. If the process consists of simple crystallization and melting there should be a wide variety of suitable composition. Why are GST and AIST the best materials?
2. Commercial DVD-RAM is stable for over 1 000 000 cycles. What makes the switching so reproducible and the media so stable?
3. GST crystallizes within 30 ns and amorphous bits can be recorded with femtosecond pulses. Why are the structural transformations so fast? Structure relaxation involving ordering of the amorphous material is likely to proceed on a longer time scale.
4. The crystallization process is characterized by an activation energy of 2–3 eV. Should the crystallization be a solid-state process, one would expect the activation energy to be on the order of the energy gap, i. e. ≈ 0.3 eV. The observed activation energy is rather reminiscent of a molecular-type excitation. Why is the activation energy so high?
5. In typical semiconductors (and in chalcogenides in particular), the amorphous phase is characterized by a smaller band gap than the crystalline phase. This is typically due to the fact that the bonds in the amorphous materials are weaker and hence the splitting between the bonding and antibonding states, which form the valence and conduction bands, respectively, is smaller. In phase-change materials the situation is reversed, namely, it is the crystalline phase that possesses a narrower band gap and higher reflectivity than the amorphous phase. What is the reason for this abnormality?
6. And, finally, what is the role of light? Although it has been tacitly assumed that light is simply heating the material, a very high concentration of nonequilibrium carriers created by intense light may—and most likely does—play a role.

In order to develop novel optical media insightfully, one has to answer the above questions. These, in turn, require detailed knowledge of the structure of the material in both the crystalline and amorphous phases as well as the atomic mechanism of the structural changes upon the phase transition.

49.1.2 Local Structure and its Changes During the Phase Transition

An ideal tool to investigate the local structure of a material and its changes on the atomic scale independent of the state of the material (crystalline or

amorphous) is X-ray absorption fine-structure (XAFS) spectroscopy.

Extended X-ray absorption fine structure (EXAFS) allows one to obtain information about the local structure around selected chemical species, such as the average coordination number, the bond lengths, the chemical nature of the neighboring species, as well as the bond-length disorder parameter, or mean-square relative displacement (MSRD). The technique is selective to the absorbing atom, which allows one to probe the local structure around different constituent elements independently.

X-ray absorption near-edge structure (XANES), which involves multiple scattering, additionally allows one to probe the local arrangement of atoms on a scale somewhat beyond the first-nearest neighbors, in particular, it is sensitive to the mutual arrangement of the neighboring atoms in space, i. e. includes bond-angle information. As XANES features are also a consequence of transitions from occupied core states to unoccupied conduction-band states, the spectra also contain information about the density of unoccupied conduction-band states. It should be mentioned that recent advances in theory have made it possible to simulate EXAFS and XANES spectra with good accuracy [49.3].

The Crystalline State

The stable crystal structure of GST is hexagonal [49.4, 5]. Thin films, however, crystallize into a different structure. Recent X-ray diffraction (XRD) studies have lead to a conclusion that thin GST layers crystallize into the rock-salt structure with Te atoms occupying sites on one face-centered cubic (fcc) sublattice with Ge and Sb randomly forming the other fcc sublattice (20% of the sites being vacant) (Fig. 49.3) [49.6, 7]. A lattice parameter of 6.02 Å was reported. The isotropic atomic displacements B_0, which is a measure of atomic displacements from the ideal crystallographic positions due e.g. to thermal vibrations, found via the fitting process were 1.2 $Å^2$ and 3.2 $Å^2$ for the Te, and Ge(Sb) species, respectively, which correspond to atomic displacements of 0.1 Å and 0.2 Å for the Te and Ge(Sb) species, respectively.

It was suggested [49.5] that the cubic structure of GST (which is rather isotropic and hence more similar to the amorphous structure than any other crystal structure)

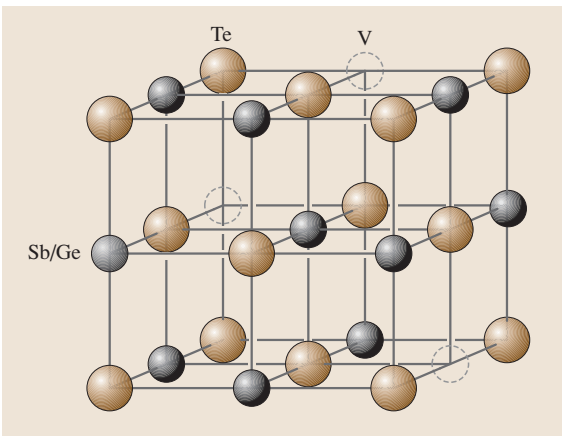

Fig. 49.3 Structure of metastable crystalline Ge–Sb–Te as suggested based upon X-ray diffraction measurements

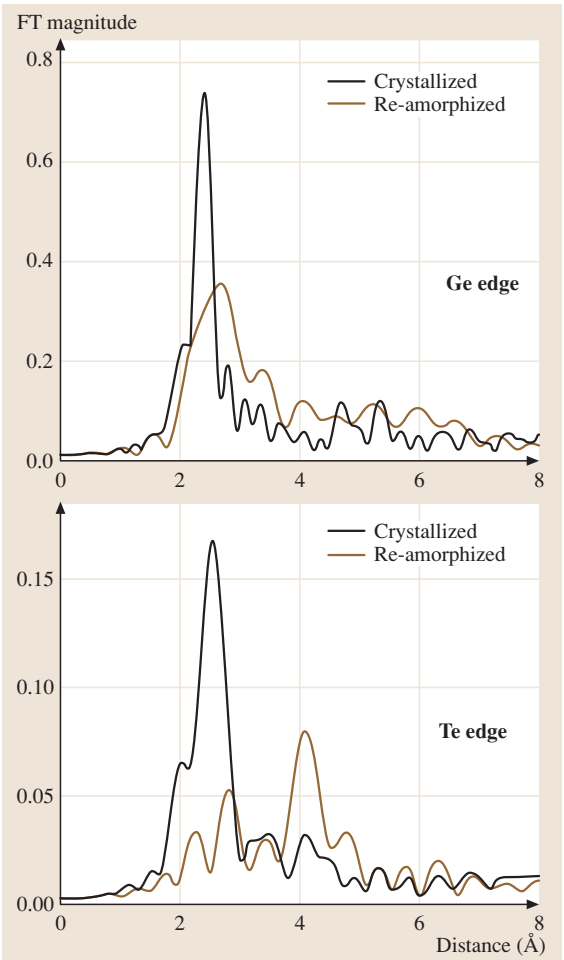

Fig. 49.4 Fourier-transformed Ge and Te K-edge EXAFS spectra of $Ge_2Sb_2Te_5$ measured for both the crystalline and amorphous states

was the reason for the high-speed switching and stable performance.

The above result gives rise to one more question. Why is B_0 so large (7% of the bond length)? In other words, is the structure really rock salt?

Below we summarize the authors' recent efforts to investigate the local structure of GST using XAFS. Measurements were performed at BL12C at the Photon Factory (Tsukuba, Japan) and BL01B1 at SPring8 (Hyogo-ken, Japan).

The Fourier-transformed (FT) spectra for the Ge and Te edges of GST are shown in Fig. 49.4. It should be noted that the r-space data shown in Fig. 49.4 are not real-space radial distribution function data but the magnitude of the Fourier transforms (FTs) of the k-space EXAFS data. The peak positions in the figure are shifted from the actual interatomic distances toward lower r because of the photoelectron phase shift $\delta(k)$ in the phase factor of the EXAFS oscillations. The spectra measured at the Sb edge did not show any significant variation between the two states and are not shown here.

Details of the data analysis can be found elsewhere [49.8]. The main results for crystalline GST are summarized below. We found two types of bond lengths, namely shorter bonds and longer bonds for both Te–Ge and Te–Sb (for Te–Ge: 2.83 ± 0.01 Å, and 3.2 ± 0.3 Å and for Te–Sb: 2.91 ± 0.01 Å and 3.2 ± 0.3 Å). It should be noted here that the observation of splitting of the bond lengths into two groups is very similar to the case of GeTe. The uncertainties for the longer bonds are rather large. For this reason no definitive conclusions could be drawn about the longer bonds and in what follows we shall exclusively concentrate on the shorter bonds. It should be noticed here that another commercially used material, AIST, also possesses subsets of shorter and longer bonds [49.9].

No Sb–Ge bonds were detected, in agreement with the fact that Sb and Ge do not intermix in the solid phase but we clearly observed a second-nearest-neighbor Te–Te peak at 4.26 Å.

It should also be mentioned that the mean-square relative displacements (MSRD) of the Te–Ge bond length obtained in EXAFS are considerably (lower (0.02 Å^2) than) the isotropic atomic displacements of single atoms obtained from XRD (0.04 Å^2). This result demonstrates that Ge and Sb atoms do not deviate from the ideal rock-salt positions in a random way but in a strongly correlated manner with respect to the neighboring Te atoms, i. e. the crystalline structure is in fact a *distorted* rock-salt-like structure similar to the case of the ferroelectric GeTe. The off-center location of the Ge atoms

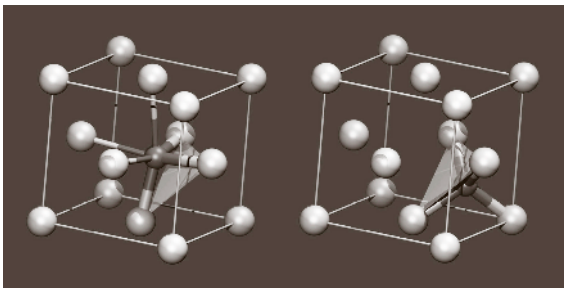

Fig. 49.5 Structural modification of GST upon transformation from the crystalline (*left*) to amorphous (*right*) state (after [49.8])

means that there is a net dipole moment and suggests that GST is a ferroelectric material [49.10].

The Amorphous State

We now turn to the amorphous state. It was found that both Te–Ge and Te–Sb bonds get *shorter* (2.61 Å and 2.85 Å, respectively) and *stronger* upon amorphization, as evidenced by Fig. 49.4. At the same time, the Te second-neighbor peak becomes considerably weaker but does not disappear completely. The MSRD value decreases from 0.02 Å^2 in the crystalline state to 0.008 Å^2 in the amorphous state.

Such a behavior is highly unusual for typical three-dimensional covalently bonded solids as, due to the anharmonicity of interatomic potentials, disordering typically results in an increase of the bond lengths and the bond-length disorder. The obtained results reminds one of the case of molecular solids where the presence of intermolecular and intramolecular bonds determines the crystallization–amorphization behavior.

In the current case, a bond-strength hierarchy also exists and the following model of structural rearrangement can be envisaged. Upon melting, the longer Te–Ge (and Te–Sb bonds) are broken and, as a result, the shorter bonds become even shorter and stronger, i. e. the amorphous phase is *locally* more ordered than the crystalline phase. Our Raman scattering experiments provided further grounds for this model, namely, the Raman measurements for both GeTe and GST [49.11] showed that the spectra for the crystalline films are dominated by a peak located at lower wavenumbers, i. e. "mode softening" takes place upon crystallization. This situation can be compared with the case of Se or Te when the interchain interaction is weakened, giving rise to a Raman peak located at higher wave number [49.12]. It should be mentioned that an increased local bond or-

der in the amorphous phase was also observed for selenium [49.13].

To get further insight into the structure of the amorphous phase, we also performed XANES simulations and found that the best agreement with experiment was obtained when Ge was allowed to acquire its preferred tetrahedral surrounding in the amorphous phase [49.8, 11].

This structural transformation is illustrated in Fig. 49.5 where a Ge atom is shown within the fcc sublattice formed by Te atoms. The Ge atoms occupy octahedral and tetrahedral symmetry positions in the crystalline and amorphous states, respectively. The stronger covalent bonds are shown with thicker lines than the weaker bonds (Fig. 49.5 left). An intense laser pulse induces rupture of the weaker bonds and the Ge atom flips into the tetrahedral position (Fig. 49.5 right). An alternative description of the structural transformation upon melting is an umbrella-flip distortion resulting in disordering of the Ge sublattice. Notice, that the three covalent bonds remain intact. This conservation of the system of stronger covalent bonds is crucial: the material is not molten in a conventional sense.

Support for the aforementioned transformation comes from an estimate of the Ge–Te distance from the crystallographic data. Using a lattice parameter of GST obtained by X-ray diffraction [49.6, 7]), the Ge–Te distance–the Ge atoms being in a tetrahedral symmetry position–can be easily calculated to be 2.61 Å, i. e. exactly the value obtained from the EXAFS analysis. This consistency between the results obtained using two different structural techniques is the ultimate proof of the suggested structural modification as well as the generality of the structural modification in GeTe-based alloys.

It is interesting to note that very similar bond lengths for the crystalline and amorphous states were also observed for the binary GeTe [49.11, 14, 15], indicating that it is the GeTe component of the quasibinary GeTe–Sb_2Te_3 that is mainly responsible for the observed phase transition.

Sb-edge XANES does not exhibit any significant changes upon amorphization (except for the Sb–Te bond shortening [49.8]) implying that the local arrangement of atoms around Sb remains essentially unchanged in accordance with the above model. We believe that the Sb atoms mainly play the role of enhancing overall stability of the metastable crystal structure by participating in the overall electron balance.

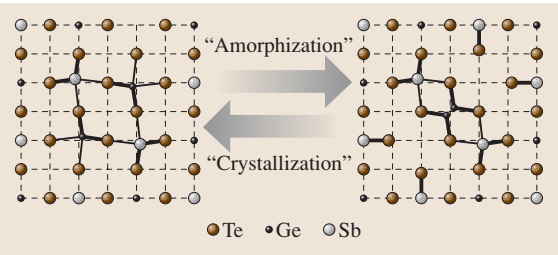

Fig. 49.6 Medium-range-order changes in GST upon crystallization–amorphization transition

Intermediate-Range-Order Changes

The structural change on an *intermediate-range-order* scale can be viewed as following (Fig. 49.6). After rupture of the weaker Ge–Te bonds the Ge atoms flip into the tetrahedral symmetry position forming the $GeTe_4$ tetrahedra. At the same time, the broken weaker Ge–Te bonds no longer counterbalance the Sb–Te bonds on the opposite site and, as a result, the Sb–Te bonds become structure-determining. The structure relaxes making the Sb–Te bonds shorter (just as in amorphous Se the intrachain bonds get shorter upon amorphization [49.13]). The Sb–Te bond shortening upon amorphization has indeed been observed experimentally [49.8]. This can be viewed as the local phase separation into GeTe and Sb_2Te_3 phases. Finally, the structure relaxation causes a distortion in the Te fcc sublattice. It is important that the amorphous phase possesses a well-defined (single-state) structure without long-range periodicity. We believe that the well-defined local structure of the amorphous state is the reason for the overall stability of the GST-based optical media.

49.1.3 Related Issues

Although it is generally assumed that the role of a laser pulse is simply to heat the material, we believe that electronic excitation creating nonequilibrium charge carriers is crucial for the weakening and subsequent rupture of the subsystem of weaker Ge–Te bonds. Indeed, the presence of longer (weaker) bonds implies that the density of states corresponding to these bonds is lower in energy and hence photogenerated nonequilibrium carriers more readily populate these states, making them more susceptible to thermal vibration-induced dissociation.

As mentioned above, another commercially used material, AIST, has a similar bond hierarchy [49.9], which allows us to suggest that the basic mechanism underlying the phase-change transition in the two groups of materials are essentially the same.

It should be stressed that this structural transformation involves a change in the hybridization from p-type bonding in the rock salt to sp^3 hybridization in the amorphous state. This substantial change in the electronic states accounts for the very large change in optical and electrical properties of GST upon the crystallization–amorphization transition.

It should also be noticed here that the unveiled structural modification can also account for why it is the crystalline regions that possess a smaller gap and higher reflectance. Indeed, the crystal structure involves both shorter and longer bonds. The longer (and hence weaker) bonds are characterized by a smaller energy splitting between the bonding and antibonding states and thus determine the positions of the valence and conduction band edges (and the width of the band gap) in the crystal. In the amorphous phase, on the other hand, the initially weaker bonds break and disappear altogether and the initially stronger bonds get even shorter and stronger. As a result, the splitting between the bonding and antibonding states increases, which produces a larger band gap and lower reflectivity compared to the crystalline phase.

49.2 Super-RENS Discs

Recent progress in multimedia requires continuously higher storage densities and faster data access. A fundamental obstacle here is the so-called diffraction limit, which does not allow one to focus the beam into a spot smaller than $\Phi > \lambda/(2\mathrm{NA})$, where Φ, λ, and NA are the laser spot diameter, light wavelength and numerical aperture (< 1.0) of the lens, respectively.

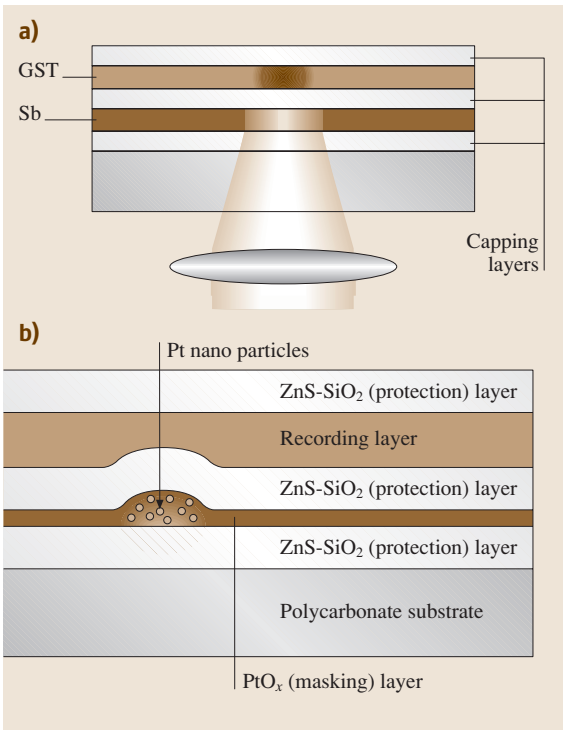

Fig. 49.7 A schematic presentation of **(a)**transmission- and **(b)**scattering-type super-RENS discs

Various approaches to tackle the problem have been suggested. The most promising among them (within optical data-storage limits) are the following: use of dual-layer disks, use of blue and blue–violet lasers (with a shorter wavelength), use of large numerical apertures, and use of the near-field technique. The latter technique allows one to avoid completely the restrictions on the dot size imposed by the diffraction.

Near-field recording is now being actively developed, following a different routes. One such route is the use of so-called super-resolution near-field structures (super-RENS) [49.16], recently developed at our center. The most important feature of this approach is that the near-field aperture is incorporated into the disk itself, i. e. the near-field recording is realized based solely on thin-film technology. Typical super-RENS structures are shown in Fig. 49.7.

As can be seen from the figure, in addition to the recording layer sandwiched between two capping layers there is a masking layer present. At the initial stages of super-RENS development the masking layer used was Sb (Fig. 49.7a). When an intense laser pulse hits the structure, the Sb layer heats up. When heated, the Sb undergoes the Peierls transition, i. e. a gap in the density of states is formed. As a result, a small aperture opens in it, which serves as a near-field light source [49.16]. The distance between the light source and the recording media is now fixed and determined by the thickness of the capping layer between the masking layer and the GST layer. With optimized parameters for each layer, the aperture in the Sb layer opens for sufficient time to record a bit into the GST layer. When the disk rotates and the exposed Sb spot moves away from the light, the aperture closes. A similar process takes place during the read-out stage.

An alternative design contains a MeO_x (Me=Ag, Pt) as the masking layer. Light that is absorbed by the recording layer generates heat and thus causes decomposition of MeO_x with the subsequent formation of Me nanoparticles within an oxygen bubble (Fig. 49.7b) [49.17]. The role of the localized plasmons excited in the nanoparticles has been discussed in detail previously [49.18]. In what follows we very briefly discuss the role of the recording layer.

There are various questions regarding the write-in and read-out mechanisms of super-RENS. In particular, in important question is how can a laser beam with a diameter of $\approx 1\,\mu m$ read out individual bits with sizes on the order of 100 nm? While there is no definite answer to this question several alternatives have been suggested. Below we describe one possibility, viz., a model based on the ferroelectric catastrophe [49.10].

As discussed earlier, GST in its metastable crystalline form possesses a net dipole moment, i. e. it is a potential ferroelectric. Ferroelectrics are known to possess a very high dielectric constant in a rather narrow temperature range close to the Curie temperature. Intense light acting upon the disk during the read-out heats the rotating disk. Because of the rotation, the temperature profile is asymmetric. There is only a rather narrow region where the temperature of the GST corresponds to the Curie temperature. It is only this region that possesses a high dielectric constant and a very high reflectivity, which enables one to read out marks whose size is considerably smaller than the laser spot [49.10].

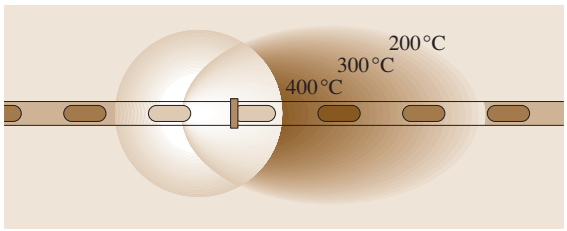

Fig. 49.8 The ferroelectric catastrophe model of super-RENS read-out

Interestingly, the other phase-change material, AIST, is also one of the best materials for use in super-RENS discs. Since both kinds of materials possess longer and shorter bonds, and hence a net dipole moment, the suggested ferroelectric-catastrophe model may operate in both cases. Experiments to further investigate the ferroelectric properties of GST and AIST and their relevance to the super-RENS read-out mechanism are currently underway.

49.3 In Lieu of Conclusion

While it took almost 40 years to elucidate the origin of the structural change behind conventional phase-change recording, we hope that progress related to understanding of the super-RENS mechanism will be achieved on a much shorter timescale. To complete this chapter, we would like to note that presently marks as small as 80 nm can be successfully recorded with a carrier-to-noise ratio (CNR) over 40 dB. The progress obtained in the field so far makes us confident that optical recording at a density higher than 100 GB/disc will become widely available in the very near future.

References

49.1 R. Ovshinsky: Phys. Rev. Lett. **21**, 1450 (1968)
49.2 T. Ohta, S. R. Ovshynsky: *Photo-Induced Metastability in Amorphopus Semiconductors*, ed. by V. Kolobov A. (Wiley-VCH, Weinheim 2003) p. 310
49.3 A. L. Ankudinov, B. Ravel, J. J. Rehr: Phys. Rev. B **58**, 7565 (1998)
49.4 I. I. Petrov, R. M. Imamov, Z. G. Pinsker: Sov. Phys. Cryst. **13**, 339 (1968)
49.5 N. Yamada, T. Matsunaga: *International Symposium on Optical Memories. Technical Digest* (Jeju, Korea 2004) p. 70
49.6 T. Nonaka, G. Ohbayashi, Y. Toriumi, Y. Mori, H. Hashimoto: Thin Solid Films **370**, 258 (2000)
49.7 N. Yamada, T. Matsunaga: J. Appl. Phys **88**, 7020 (2000)
49.8 A. V. Kolobov, P. Fons, A. I. Frenkel, A. L. Ankudinov, J. Tominaga, T. Uruga: Nature Mater. **3**, 703 (2004)
49.9 T. Matsunaga, Y. Umetani, N. Yamada: Phys. Rev. B **64**, 184116 (2001)
49.10 J. Tominaga, T. Shima, M. Kuwahara, T. Fukaya, A. V. Kolobov: Nanotechnology **15**, 411 (2004)
49.11 A. V. Kolobov, P. Fons, J. Tominaga, A. L. Ankudinov, S. Yannopoulos: J. Phys.: Condens. Matter **16**, S5103 (2004)

49.12 M. H. Brodsky: *Light Scattering in Solids*, ed. by M. Cardona (Springer, Berlin Heidelberg New York 1983) p. 205

49.13 D. E. Sayers: Structural Studies of Disordered Systems using EXAFS. In: *Proc. 7th Int. Conf. Amorph. and Liquid Semicond.*, ed. by W. E. Spear (University of Edinburgh, Edinburgh 1977) p. 61

49.14 A. V. Kolobov, P. Fons, J. Tominaga: Appl. Phys. Lett. **82**, 382 (2003)

49.15 Y. Maeda, M. Wakagi: Jpn. J. Appl. Phys. **30**, 101 (1991)

49.16 J. Tominaga, T. Nakano, N. Atoda: Appl. Phys. Lett. **73**, 2078 (1998)

49.17 T. Kikukawa, T. Nakano, T. Shima, J. Tominaga: Appl. Phys. Lett. **81**, 4697 (2002)

49.18 J. Tominaga, D. P. Tsai (Eds.): *Optical Nanotechnology: The Manipulation of Surface and Local Plasmons*, ed. by J. Tominaga, D. P. Tsai (Springer, Berlin Heidelberg New York 2003) p. 212